Structural curvature versus amplitude curvature

Satinder Chopra, Arcis Seismic Solutions, Calgary, Canada
Kurt J. Marfurt, University of Oklahoma, Norman, USA

Because they are second-order derivatives, seismic curvature attributes can enhance subtle information that may be difficult to see using first-order derivatives such as the dip magnitude and the dip-azimuth attributes. As a result, these attributes form an integral part of most seismic interpretation projects. This conventional computation of curvature may be termed as *structural curvature*, as lateral second-order derivatives of the structural component of seismic time or depth of reflection events are used to generate them. In this study, we explore the case of applying lateral second-order derivatives on the amplitudes of seismic data along the reflectors. We refer to such computation as *amplitude curvature*. For volumetric structural curvature we compute first derivatives in the inline and crossline components of structural dip. For amplitude curvature, we apply a similar computation to the inline and crossline components of the energy-weighted amplitude gradients, which represent the directional measures of amplitude variability. Because of limits to lateral resolution, application of amplitude curvature computation to real seismic data results in greater lateral resolution than structural curvature. The images are mathematically independent of each other and thus highlight different features in the subsurface, but are often correlated through the underlying geology.

Since the introduction of the seismic curvature attributes by Roberts (2001), curvature has gradually become popular with interpreters, and has found its way into most commercial software packages. Curvature is a 2D second-order derivative of time or depth structure, or a 2D first-order derivative of inline and crossline dip components. As a derivative of dip components, curvature measures subtle lateral and vertical changes in dip that are often overpowered by stronger, regional deformation, such that a carbonate reef on a 20° dipping surface gives rise to the same curvature anomaly as a carbonate reef on a flat surface. Such rotational invariance provides a powerful analysis tool that does not require first picking and flattening on horizons near the zone of interest. Roberts introduced curvature as a 2D second-derivative computations of picked seismic surfaces. Soon afterward, Al-Dossary and Marfurt (2006) showed how such computations can be computed from volumetric estimates of inline and crossline dip components. By first estimating the volumetric reflector dip and azimuth that best represents the best single dip for each single sample in the volume, followed by computation of curvature from adjacent measure of dip and azimuth, a full 3D volume of curvature values is produced.

To clarify our subsequent discussion, we denote the above calculations as structural curvature, the (explicit or implicit) lateral second derivatives of reflector time or depth. Many processing geophysicists focused on statics and velocity analysis think of seismic data as composed of amplitude and phase components, where the phase associated with any time t and frequency f is simply $\phi = 2\pi ft$. Indeed, several workers have

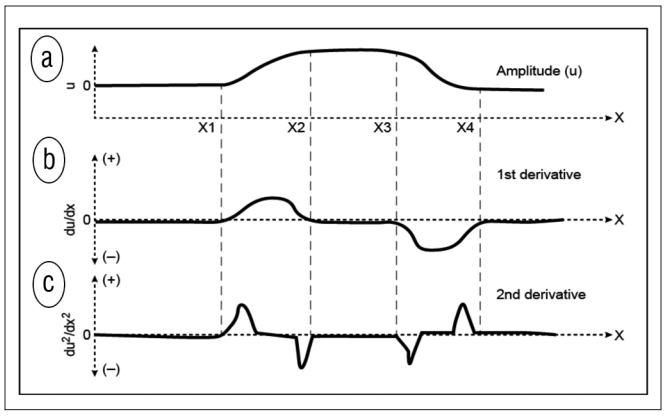

Figure 1. *Effect of the first and second derivatives on a one-dimensional amplitude profile. The two extrema seen in (c) show the limits of the amplitude anomaly.*

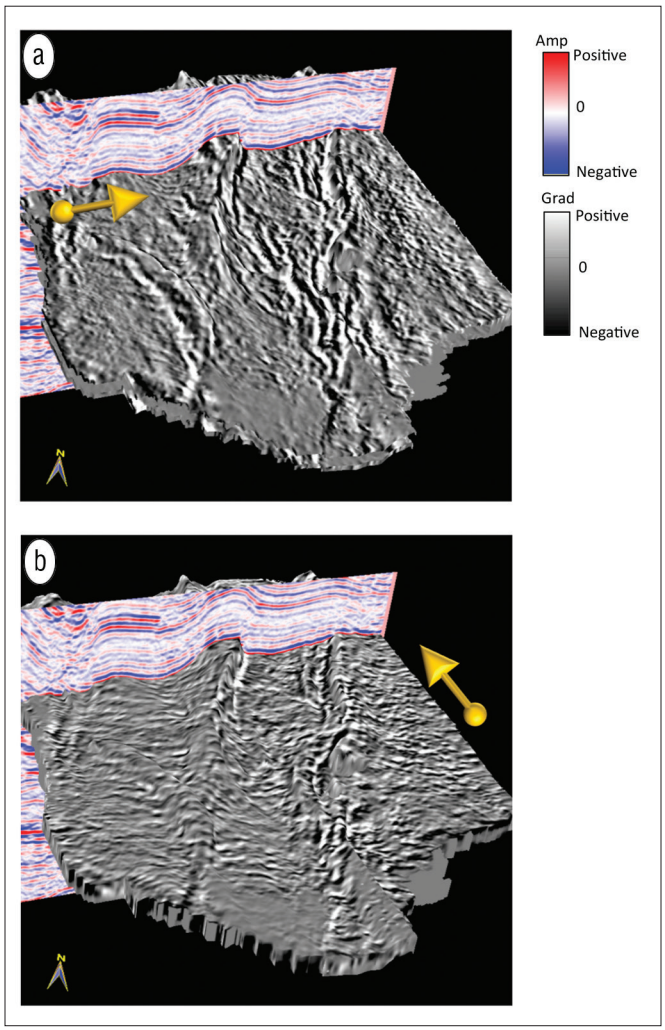

Figure 2. *3D chair view showing the seismic inlines correlated with the (a) inline energy gradient, and (b) the crossline energy gradient strat cubes. The size of the 3D volume is about 100 km², and 1 s of seismic data is shown on the vertical display.*

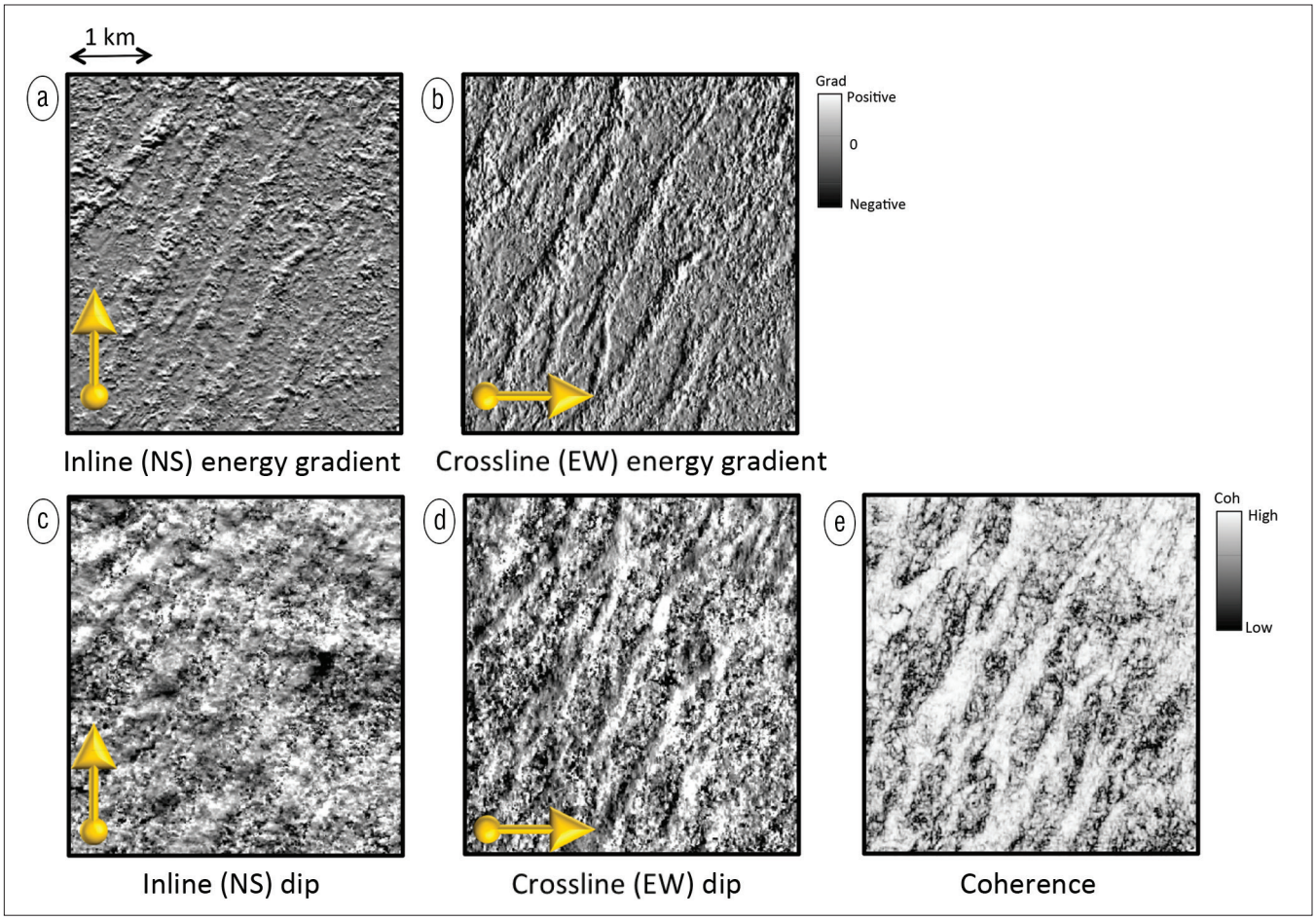

Figure 3. *Stratal slices close to 900 ms from (a) inline (NS) energy gradient, (b) crossline (EW) energy gradient, (c) inline (NS) dip, (d) crossline (EW) dip, and (e) coherence attribute volumes. Notice the energy gradient displays (a and b) look sharper than their corresponding dip computation displays (c and d), and look closer to the coherence attribute display (e). Data courtesy of Fairborne Energy Ltd., Calgary.*

used the lateral change in phase as a means to compute reflector dip (e.g., Barnes, 2000; Marfurt and Kirlin, 2000).

We can also compute second derivatives of amplitude. Horizon-based amplitude curvature is in the hands of most interpreters. First, we generate a horizon slice through a seismic amplitude, rms amplitude, or impedance volume. Next, we compute the inline ($\partial a/\partial x$) and crossline ($\partial a/\partial y$) derivatives of this map. Such maps can often delineate the edges of bright spots, channels, and other stratigraphic features at any desired direction, θ ($\cos\theta\,\partial a/\partial x + \sin\theta\,\partial a/\partial y$). A common edge-detection algorithm is to compute the Laplacian of a map (though more of us have probably applied this filter to digital photographs than to seismic data),

$$e_{mean} = \frac{1}{2}\nabla^2 a = \frac{1}{2}\left(\frac{\partial^2 a}{\partial x^2} + \frac{\partial^2 a}{\partial y^2}\right). \quad (1)$$

Equation 1 is the formula for the mean amplitude curvature. Figure 1 shows a diagram of an amplitude anomaly exhibiting lateral change in one direction, x. Thereafter, we compute the first and second spatial derivatives of the amplitude with respect to x and show the results in Figures 1b and 1c. Notice the extrema seen in Figure 1c demarcate the limits of the anomaly.

Luo et al. (1996) developed an excellent edge detector similar to a scaled Sobel filter that is approximately

$$c_{Sobel} = \frac{\sum_{k=-K}^{+K}\left(\left[\frac{\partial a}{\partial x}\right]^2 + \left[\frac{\partial a}{\partial y}\right]^2\right)}{\sum_{k=-K}^{+K}\sum_{j=1}^{J} a_{jk}^2} \quad (2)$$

where the derivatives are computed in a $-K$ to $+K$ vertical sample, J-trace analysis window oriented along the dipping plane and the derivatives are evaluated at the center of the window. Radovich and Oliveros (1998) developed an early version of the "amplitude" family of curvature as applying a Laplacian operator to the logarithm of the complex trace envelope along time slices.

Marfurt and Kirlin (2000) and Marfurt (2006) showed how one can compute accurate estimates of reflector amplitude gradients, **g**, from the KL-filtered (or principal component of the data) within an analysis window:

$$g_x = \lambda_1 \sum_{k=-K}^{+K} \frac{\partial v_1(x,y)}{\partial x}, \text{ and}$$
$$g_y = \lambda_1 \sum_{k=-K}^{+K} \frac{\partial v_1(x,y)}{\partial y}, \quad (3)$$

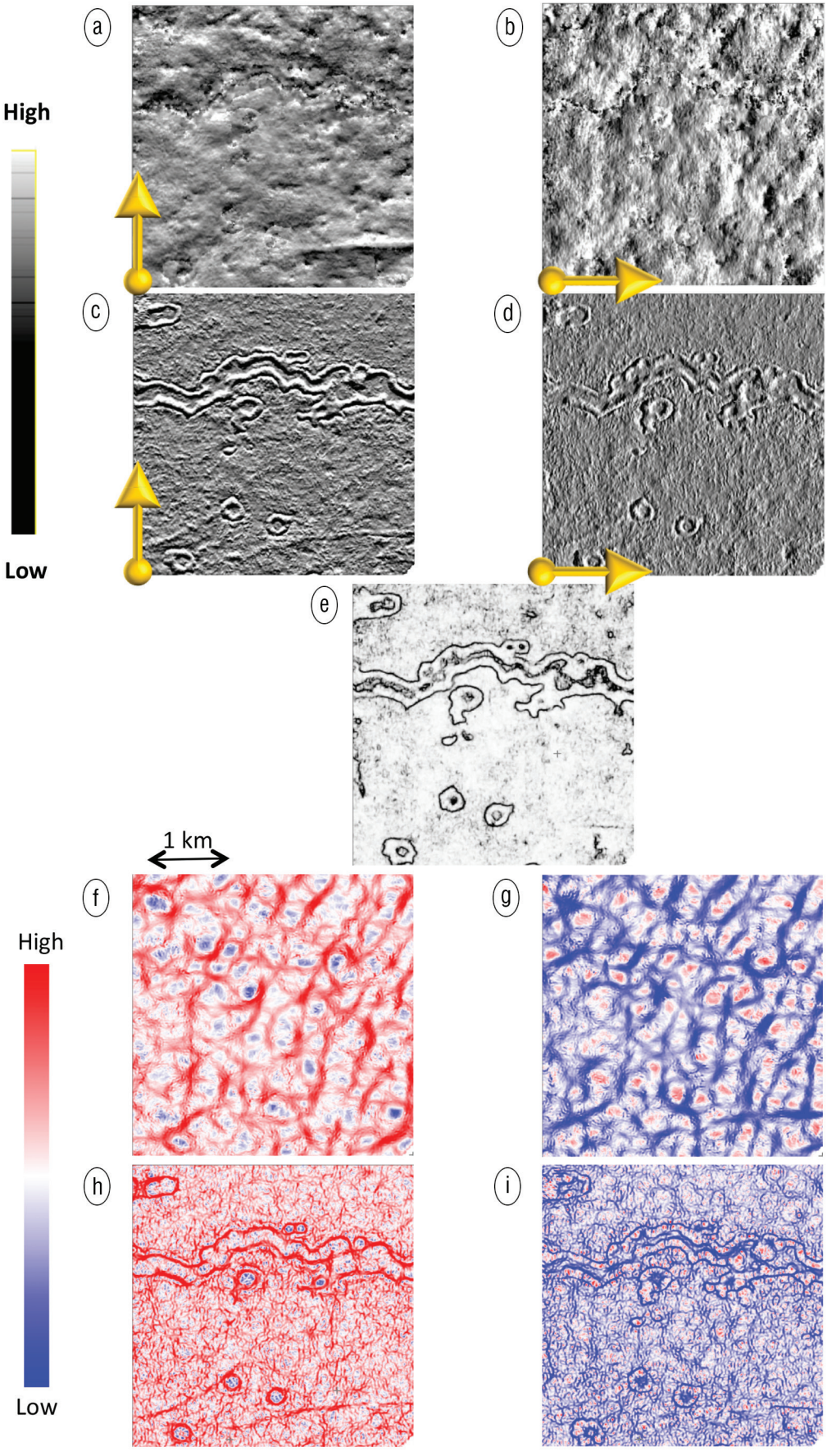

Figure 4. *Strat-slices from the (a) inline (NS) dip, (b) crossline (EW) dip (c) inline (NS) energy gradient, (d) crossline (EW) energy gradient (e) coherence, (f) principal structural positive curvature (LW), (g) principal structural negative curvature (LW), (h) principal amplitude positive curvature (LW), (i) principal amplitude negative curvature (LW). Notice the clear definition of the Winnepogsis reef boundaries, first seen better on the energy gradient volumes over the traditional inline and crossline dip volumes, and then on the amplitude curvature displays over structural curvature displays. Data courtesy of Fairborne Energy Ltd., Calgary.*

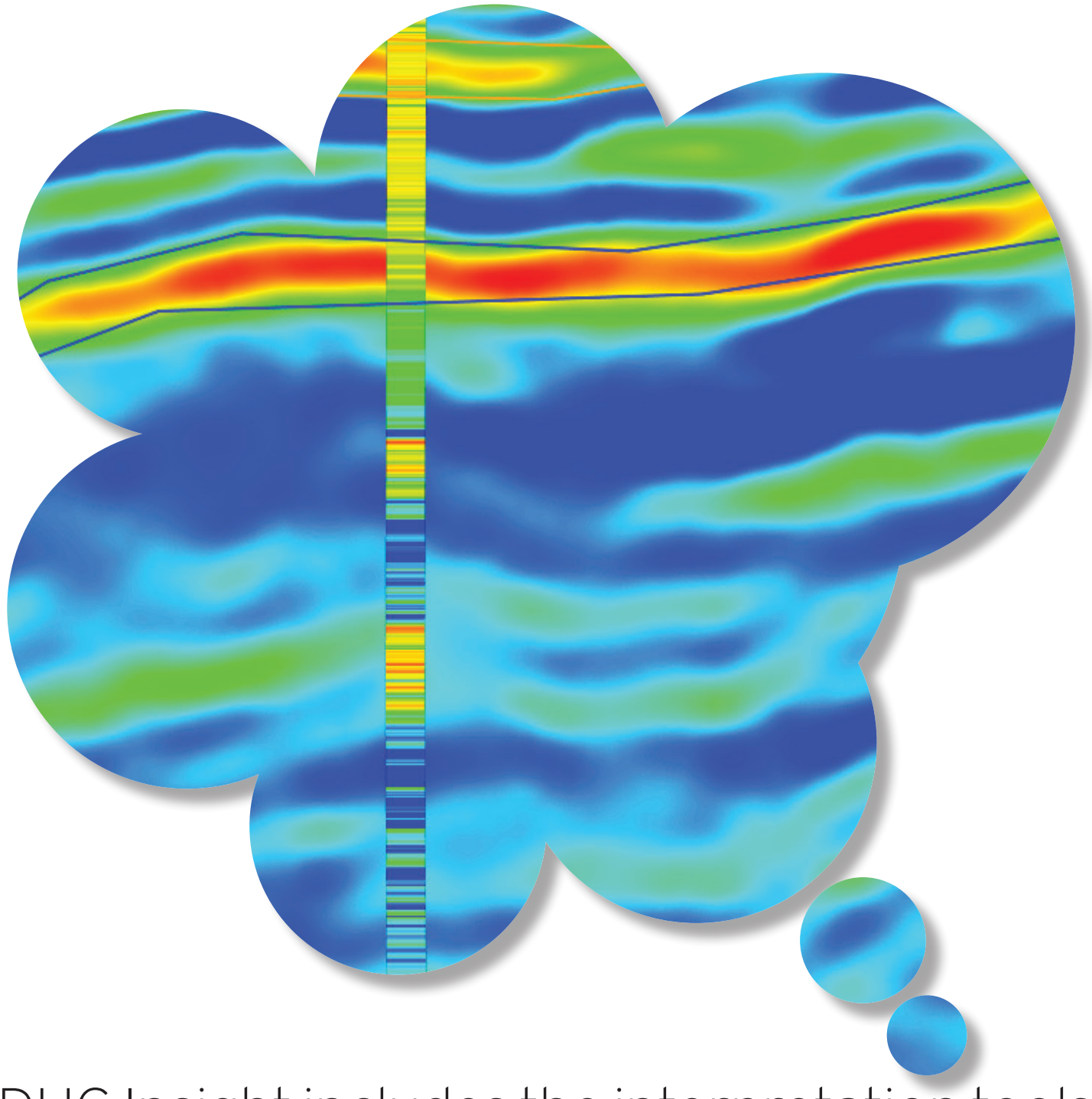

DUG Insight includes the interpretation tools you've been dreaming of.

Over 500 users worldwide are now taking advantage of DUG Insight's integrated interpretation and visualisation tools. You'll get a comprehensive range of features which include a state-of-the-art waveform propagator, flexible manual picking and fault tessellation - all of which also work seamlessly in the pre-stack domain.

Take a look for yourself and download a free 30-day trial copy from our website. Dreams really can become reality.

Download your FREE DUG Insight trial at **www.dugeo.com**

dug insight

software for the hardcore. www.dugeo.com

DownUnder GeoSolutions

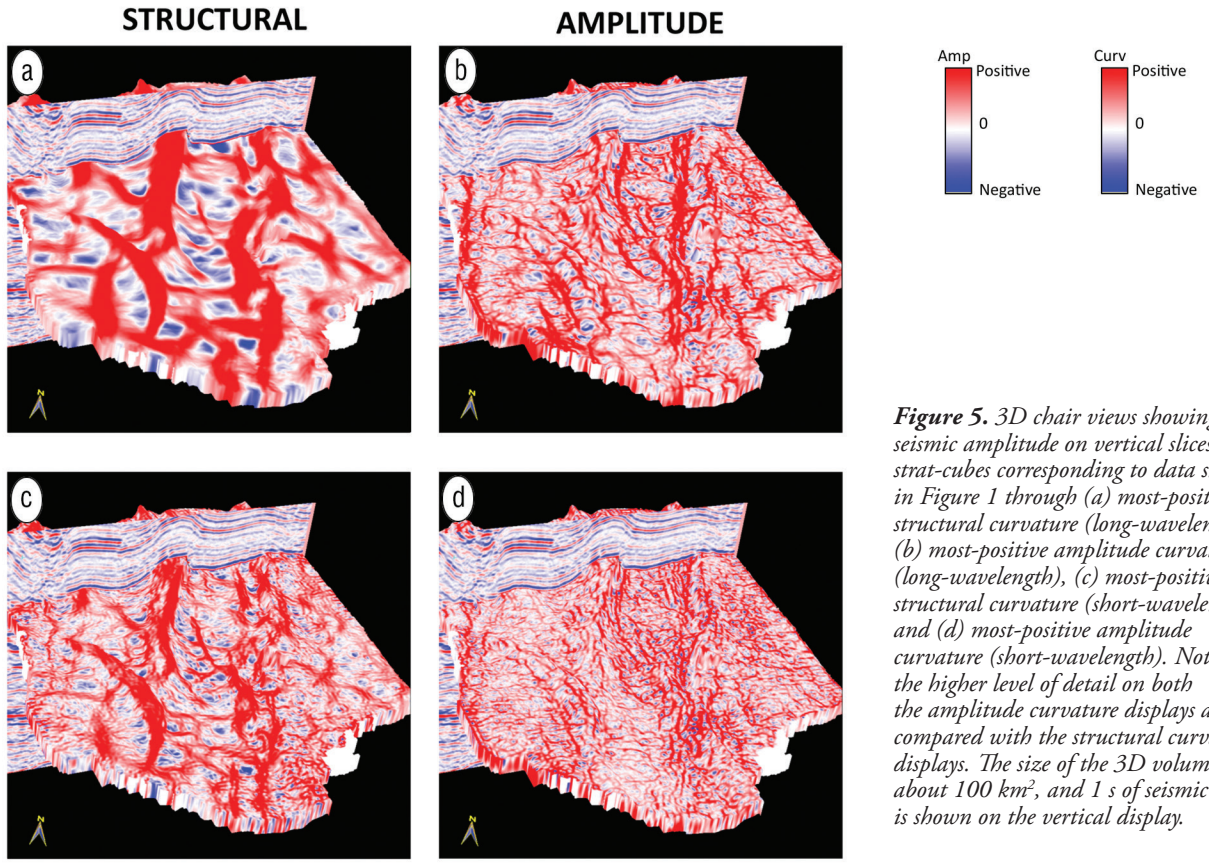

Figure 5. *3D chair views showing seismic amplitude on vertical slices and strat-cubes corresponding to data shown in Figure 1 through (a) most-positive structural curvature (long-wavelength), (b) most-positive amplitude curvature (long-wavelength), (c) most-positive structural curvature (short-wavelength), and (d) most-positive amplitude curvature (short-wavelength). Notice the higher level of detail on both the amplitude curvature displays as compared with the structural curvature displays. The size of the 3D volume is about 100 km^2, and 1 s of seismic data is shown on the vertical display.*

where $\mathbf{v}_1$ is the principal component or eigenmap of the *J*-trace analysis window, and λ_1 is its corresponding eigenvalue, which represents the energy of this data component.

In Figures 2a and b, we show a 3D chair view that correlates a vertical slice through the seismic amplitude volume and stratal slices through the inline and crossline dip and amplitude gradient volumes. All four images express independent views of the same geology (almost NS-oriented main faults and fault related fractures) as two orthogonal shaded illumination maps. In Figure 3, we compare strata slices from the inline and crossline energy gradient attributes with the equivalent slices from the inline and crossline dip and coherence attributes. Notice the energy gradient displays (Figure 3a and Figure 3b) look sharper than their corresponding dip attribute displays (Figure 3c and Figure 3d), and appear to be closer to the coherence attribute display in (Figure 3e).

For volume computation of structural curvature, the equations applied to the components of reflector dip and azimuth in the inline and crossline directions are given by Al-Dossary and Marfurt (2006). In the case of amplitude computation of curvature, the same equations could be used by applying them to the inline and crossline components of energy-weighted amplitude gradients which represent the directional measures of amplitude variability. In Figure 4, we again compare the inline and crossline dip-component attributes with their equivalent energy gradient displays and coherence. Also in the same figure, we include an equivalent comparison of the structural and amplitude curvature displays and notice that the definition of the Winnepegosis reef boundaries are sharper and more distinct on the energy gradient displays and amplitude curvature displays.

Geologic structures often exhibit curvature of different wavelengths and so curvature images of different wavelengths provide different perspectives of the same geology. Al-Dossary and Marfurt introduced the volumetric computation of long- and short-wavelength curvature measures from seismic data.

Many applications of such multispectral estimates of curvature from seismic data have been demonstrated by Chopra and Marfurt (2007a, 2007b, 2010). Short-wavelength curvature often delineates details with intense highly localized fracture systems. Long-wavelength curvature on the other hand enhances subtle folds and flexures on a scale of 100–200 traces that are difficult to see on conventional seismic data, but are often correlated to fracture zones that are below seismic resolution as well as to collapse features and diagenetic alterations that result in broader bowls.

Figure 5 and Figure 6 compare the long- and short-wavelength computation of most-positive and most-negative amplitude and structural curvature measures. In Figure 5, we notice that for both long and short wavelengths, the amplitude curvature estimates provide additional information. Structural most-positive curvature displays in Figure 5a and Figure 5c show lower-frequency detail as compared with their equivalent amplitude curvature displays in Figure 5b and Figure 5d. Similarly, Figure 6b and Figure 6d exhibit much greater lineament detail on the amplitude most-negative cur-

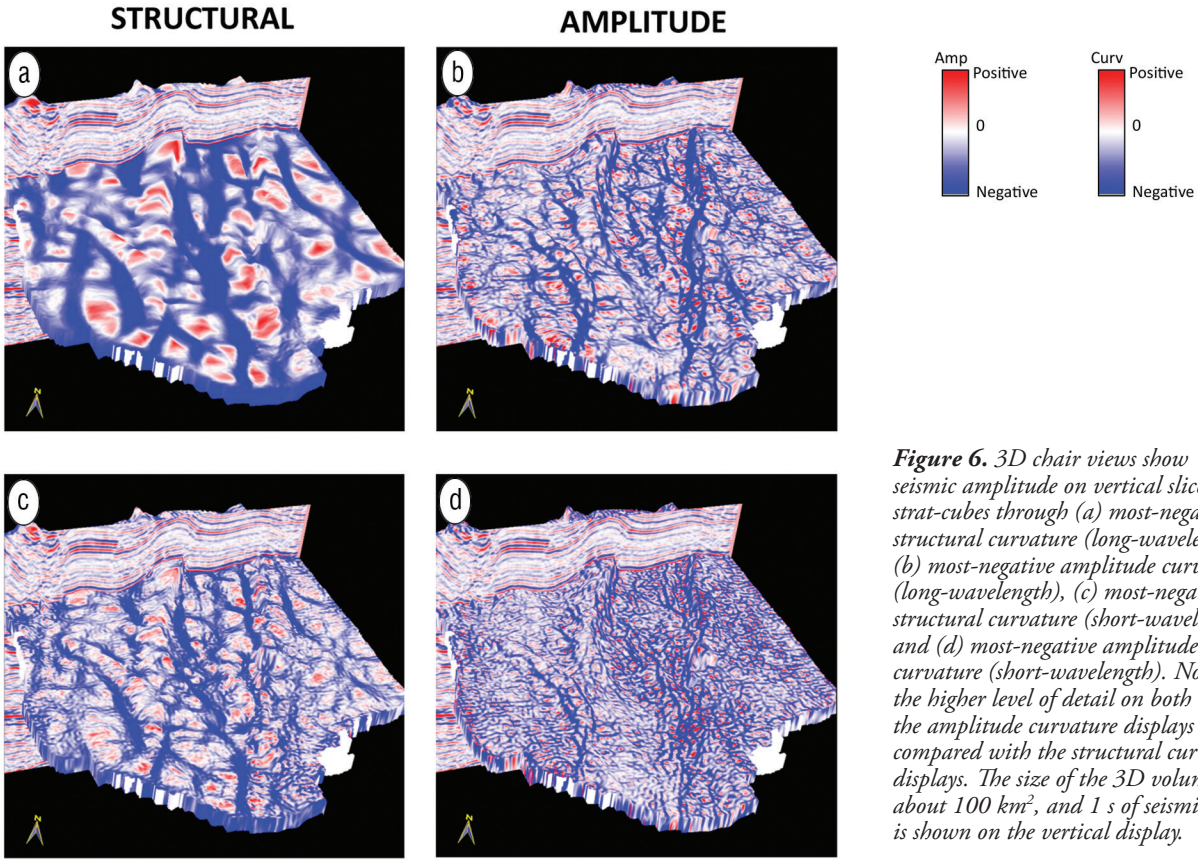

Figure 6. *3D chair views show seismic amplitude on vertical slices and strat-cubes through (a) most-negative structural curvature (long-wavelength), (b) most-negative amplitude curvature (long-wavelength), (c) most-negative structural curvature (short-wavelength), and (d) most-negative amplitude curvature (short-wavelength). Notice the higher level of detail on both the amplitude curvature displays as compared with the structural curvature displays. The size of the 3D volume is about 100 km^2, and 1 s of seismic data is shown on the vertical display.*

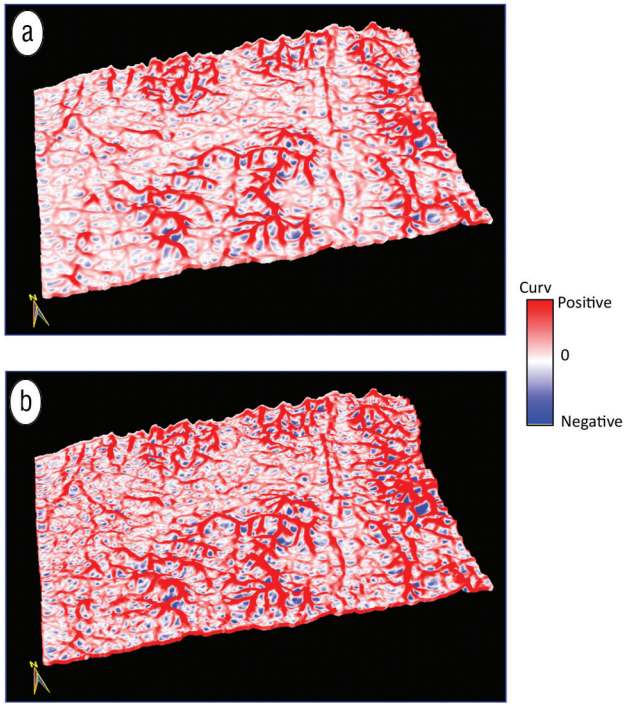

Figure 7. *Stratal slices from most-positive structural volumes computed from (a) seismic amplitude, and (b) corresponding model-driven impedance. Notice more focused lineament detail seen in (b) compared with (a). The curvature data have a size of about 250 km^2.*

vature displays than what is seen on structural most-negative curvature displays in Figure 6a and Figure 6c.

Chopra (2001) demonstrated that coherence run on impedance rather than amplitude can yield superior images. This improvement is due to the improved bandwidth and noise suppression provided by careful model-based inversion. Similarly, Guo et al. (2010) applied "amplitude" curvature to a model-based impedance volume computed over the Woodford Shale and found that low-impedance lineaments seen on most-negative amplitude curvature volumes were tightly correlated to fractures and faults in the underlying Hunton limestone. Figure 7 and Figure 8 are a similar computation applied to two surveys acquired in the Western Canadian Sedimentary Basin. Note the more focused lineament detail on curvature computed from impedance data over structural curvature computed from seismic amplitude data.

Conclusions

For data processed with an amplitude-preserving sequence, lateral variations in amplitude are diagnostic of geologic information such as changes in porosity, thickness, and /or lithology. Computation of curvature on amplitude, envelope, or impedance enhances such lateral anomalies. Curvature values are related to eigenvalues of a 2D (in this case) that measure the rate of amplitude variation in two orthogonal (or principal curvature) directions. The corresponding eigenvectors can be used to describe the strike of such lineaments,

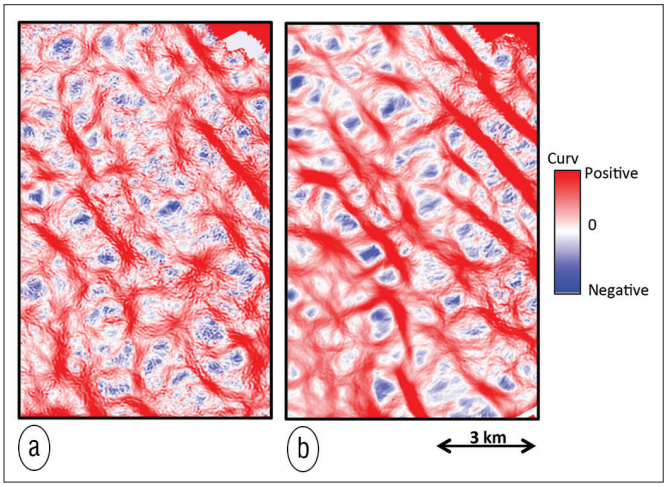

Figure 8. *Time slices through from most-positive curvature volumes computed from (a) seismic amplitude, and (b) corresponding model-driven impedance. Notice more focused lineament detail seen in (b) compared to (a).*

providing a means to azimuthally filter them into subsets for further statistical analysis or visual correlation with rose diagrams obtained from image logs. Such exercises will lend confidence in the application of amplitude curvature in seismic data interpretation. TLE

References

Al-Dossary, S. and K. J. Marfurt, 2006, Multispectral estimates of reflector curvature and rotation: Geophysics, **71**, no. 5, P41–P51, http://dx.doi.org/10.1190/1.2242449.

Barnes, A. E., 2000, Weighted average seismic attributes: Geophysics, **65**, no. 1, 275–285, http://dx.doi.org/10.1190/1.1444718.

Chopra, S., 2001, Integrating coherence cube imaging and seismic inversion: The Leading Edge, **19**, no. 4, 354–362, http://dx.doi.org/10.1190/1.1438948.

Chopra, S. and K. J. Marfurt, 2007a, Seismic attributes for prospect identification and reservoir characterization: SEG.

Chopra, S. and K. J. Marfurt, 2007b, Curvature attribute applications to 3D seismic data: The Leading Edge, **26**, no. 4, 404–414, http://dx.doi.org/10.1190/1.2723201.

Chopra, S. and K. J. Marfurt, 2010, Integration of coherence and curvature images: The Leading Edge, **29**, no. 9, 1092–1107, http://dx.doi.org/10.1190/1.3485770.

Guo, Y., K. Zhang, and K. J. Marfurt, 2010, Seismic attribute illumination of Woodford Shale faults and fractures, Arkoma Basin, OK: 80th Annual International Meeting, SEG, Expanded Abstracts, 1372–1376, http://dx.doi.org/10.1190/1.3513097.

Luo, Y., W. G. Higgs, and W. S. Kowalik, 1996, Edge detection and stratigraphic analysis using 3-D seismic data: 66th Annual International Meeting, SEG, Expanded Abstracts, 324–327, http://dx.doi.org/10.1190/1.1826632.

Marfurt, K. J. and R. L. Kirlin, 2000, 3D broadband estimates of reflector dip and amplitude: Geophysics, **65**, no. 1, 304–320, http://dx.doi.org/10.1190/1.1444721.

Marfurt, K. J., 2006, Robust estimates of reflector dip and azimuth: Geophysics, **71**, no. 4, P29–P40, http://dx.doi.org/10.1190/1.2213049.

Radovich, B. J. and R. B. Oliveros, 1998, 3D sequence interpretation of seismic instantaneous attributes from the Gorgon Field: The Leading Edge, **17**, no. 9, 1286–1293, http://dx.doi.org/10.1190/1.1438125.

Roberts, A., 2001, Curvature attributes and their application to 3D interpreted horizons: First Break, **19**, no. 2, 85–99, http://dx.doi.org/10.1046/j.0263-5046.2001.00142.x.

Acknowledgments: We thank Arcis Seismic Solutions, Calgary, for permission to show the data examples as well as for the permission to publish this work.

Corresponding author: SChopra@arcis.com

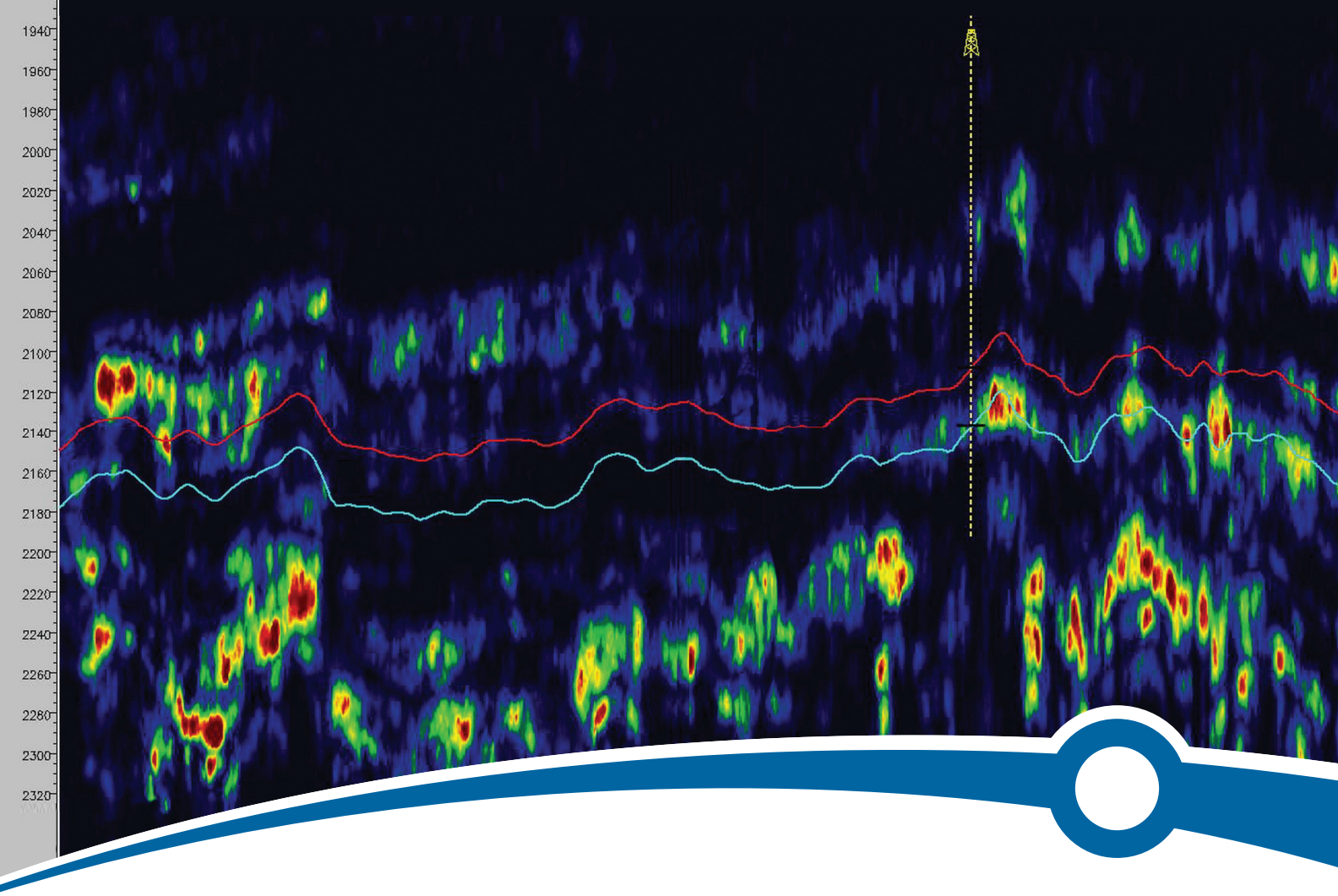

Looking for **Fractures?**

Detect fracture corridors and faults using conventional seismic data.

Want to learn more about Diffraction Imaging? Contact us!

geomage

Americas: +1-832-767-5918
Europe: +44-2070-431192
Russia and CIS: +7-499-1977517

WWW.GEOMAGE.COM
Follow us on: